IEEE Access
Multidisciplinary | Rapid Review | Open Access Journal

Received April 7, 2017, accepted April 25, 2017, date of publication May 19, 2017, date of current version June 27, 2017.

Digital Object Identifier 10.1109/ACCESS.2017.2706300

On the Placement of On-Body Antennas for Ultra Wideband Capsule Endoscopy

JAN-CHRISTOPH BRUMM, (Student Member, IEEE), AND GERHARD BAUCH, (Fellow, IEEE)
Institute of Communications, Hamburg University of Technology, 21073 Hamburg, Germany

Corresponding author: Jan-Christoph Brumm (jan.brumm@tuhh.de)

This work was supported by the German Research Foundation (DFG) and the Hamburg University of Technology (TUHH) in the funding programme "Open Access Publishing."

ABSTRACT Ultra wideband communication is proposed as an alternative to increase the data rate for in-body to on-body communication compared with existing narrowband standards. However, up to now, it is unknown, which maximum data rates can be achieved in this environment. The channel capacity is a theoretic tool that allows quantifying this limit. In a frequency-dependent environment like the human body, it is necessary to know the frequency dependence of the communication channel to calculate the channel capacity. As there are no reproducible models available in literature that enable the calculation of the channel capacity, we propose a new channel modeling technique based on a plane wave propagating through a multi-layered dielectric. From this simplified model, the frequency-dependent path loss for various in- and on-body locations can be calculated analytically. Thus, the channel capacity can be determined. In addition, this approach offers the possibility to determine the optimum position of multiple receive antennas on the abdominal surface. Results show that a single receive antenna gives nearly no improvement compared to existing standards. However, if the number of antennas is increased to 5, the 10%-outage capacity can be improved by several orders of magnitude.

INDEX TERMS Ultra wideband communication, in-body communication, capsule endoscopy, propagation losses, channel capacity, diversity reception.

I. INTRODUCTION

Capsule endoscopes provide an alternative to classical endoscopy as they can reach the small intestine. These capsules are usually equipped with one or two cameras, a battery and a radio transmitter. They have a size of not more than 11 mm × 26 mm [1]. The pictures taken by the camera are transmitted wirelessly to an on-body receiving device. Existing capsules mostly use the Medical Implant Communication Service (MICS) band from 402 MHz to 405 MHz [1]. The allowed bandwidth in this frequency range is restricted to 300 kHz, which means that the maximum achievable data rate is limited, e.g., the IEEE 802.15.6 standard for in-body communication standardizes a data rate of up to 455.4 kbit/s in the MICS band [2].

Due to the limited data rate, the resolution and the frame rate of the transmitted images are restricted. Today's capsule endoscopes have a resolution of at most 320 × 320 pixels [1]. To give the physicians the possibility for more confident diagnoses it is desirable to increase the image resolution and the frame rate to avoid blind spots inside the gastrointestinal tract.

Increasing the data rate requires a higher modulation order if the bandwidth is to be kept constant. To achieve the same bit error rate with a higher order modulation the transmit power would need to be increased. However, increasing the transmit power is not a desirable option, as the transmit power should always be kept as small as possible to avoid adverse health effects. Additionally, the transmit power is limited by the specific absorption rate limits given by the International Commission on Non-Ionizing Radiation Protection (ICNIRP) in [3]. The usage of ultra wideband communication allows for a much higher bandwidth. Hence, the data rate could be increased without having to increase the transmit power compared to communication in the MICS band.

Ultra wideband (UWB) communication is allowed in the range of 3.1 GHz to 10.6 GHz for transmit signals with a bandwidth greater than 500 MHz and an equivalent isotropically radiated power spectral density of less than −41.3 dBm/MHz [4]. In addition to the higher bandwidth it is possible to build much smaller and simpler

transmitters for UWB communication compared to narrowband communication [5].

To the best of our knowledge there exist no publications that investigate the channel capacity of ultra wideband in-body communication in the abdominal region. The channel capacity is a theoretical upper limit on the data rate that can be transmitted over a given communication channel. For the derivation it is assumed that infinitely long sequences are transmitted with a Gaussian symbol alphabet. This is not achieved in practical applications. Nevertheless, the channel capacity gives valuable insight into the maximum achievable data rates, as for successful error correction, the data rate may never be higher than the channel capacity.

To investigate the transmission behavior of ultra wideband communication links, a suitable channel model is needed for simulation and calculation of the channel capacity. There are channel models for in-body ultra wideband communication in the abdominal region available in literature, e.g. in [6], [7], and [8]. In these studies mostly finite-difference time-domain (FDTD) simulations of the electromagnetic wave propagation were done. Additionally, there are some experimental results reported in [9] and [10].

Nearly all of these studies resulted in distance dependent path loss models only. However, the propagation properties of human tissue are frequency dependent and this should also be reflected in such a model, especially if a bandwidth of more than 500 MHz is used, as it is the case for ultra wideband transmission. Støa *et al.* [7] derived a statistical impulse response model in addition to a path loss model. Unfortunately, their model has some plausibility problems.[1]

As it is not possible to calculate the channel capacity in a frequency dependent channel without the knowledge of the frequency dependency of the path loss, a new channel modeling approach is presented in the following.

The general idea is taken from [11], where the transmission of electromagnetic waves inside the human body is modeled with the help of a multi-layered dielectric. With this simplification the frequency dependent path loss of the human tissue can be calculated analytically using results from transmission line theory. In [11] the formulas for the frequency dependent path loss of a plane electromagnetic wave passing through a multi-layered dielectric are derived. Additionally, experiments were performed, which show that the analytically predicted path loss matches well with the experimental results.

In this paper the formulas from [11] are used to calculate the frequency dependent path loss for multiple possible transmitter and receiver combinations in and on the body. The resulting frequency dependent path loss will be used to determine the channel capacity. Furthermore, it will be investigated how multiple receive antennas on the body surface can increase the channel capacity and where to place the antennas on the abdominal surface for optimum reception.

In our model a plane wave is propagating perpendicular to the tissue boundaries through the tissue layers. Thus, only reflections that occur orthogonal to the boundaries are considered. Scattering effects in any other directions are neglected. Moreover, antenna effects will not be included in our calculations, as we are interested only in the limit of the data rate imposed by the channel conditions. Both simplifications will lead to a path loss which is – as shown later in this work – on average lower than predicted with other models. However, as we are interested in the channel capacity, which is an upper bound on the data rate, these two assumptions will only loosen this bound. Nevertheless, it will remain an upper bound to what is achievable in practical applications.

An additional advantage of this simplified setup is that it is possible to investigate much more transmitter-receiver pairs compared to commonly used finite-difference time-domain (FDTD) simulations. In FDTD simulations usually only a couple of hundred communication links are investigated due to the high computational complexity. With our model it is possible to investigate several hundred thousand links in a reasonable time frame. Hence, the statistical characteristics of in-body communication can be captured much better.

The remainder of this paper is organized as follows. Section II describes the channel modeling setup and the assumptions made. In Section III the formulas for the frequency dependent path loss of a plane wave propagating through a multi-layered dielectric are derived. Section IV gives a brief derivation of the channel capacity in a frequency selective channel. In Section V the path loss of our model is compared to path loss models and experiments from literature to validate our results. Finally, in Section VI the results of the capacity calculation are presented and it is shown how to position the receive antennas optimally. Section VII concludes the paper.

II. CHANNEL MODELING SETUP

A. PREREQUISITES AND ASSUMPTIONS

To model the human body, we use the Visible Human body model provided by the Helmholtz Zentrum München [12]. The model consists of a 3D matrix indicating the position of the different human tissues inside the body. Each element of this matrix (each voxel) has a resolution of 0.91 mm × 0.94 mm × 5 mm. Fig. 1 shows one slice viewed from top and the view from the right side onto the body.

To model the propagation inside the human body with the help of a multi-layered dielectric, the complex heterogeneous structure of the human body needs to be mapped to multiple tissue layers. In [11] only one example of a connection inside the abdominal region is investigated. We extend this approach by using multiple transmitter locations in the gastrointestinal tract as well as multiple receiver locations on the abdominal surface. For each of these transmitter-receiver

[1] The propagation delays obtained from their proposed Gaussian distribution may require that the electromagnetic waves travel with a speed higher than the speed of light in human tissue.

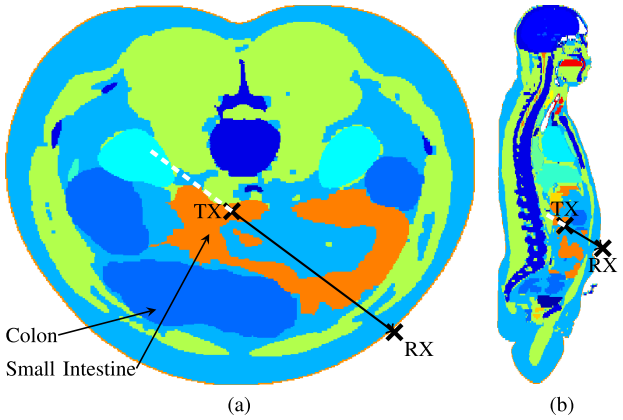

FIGURE 1. The Visible Human voxel body model. (a) View of one slice from top. (b) View from the right side. One possible transmitter location inside the gastrointestinal tract is marked with TX. A possible receive antenna location on the body surface is marked with RX. The tissues along the black line are mapped to a multi-layered dielectric modeling the link from TX to RX. To calculate the source impedance for this link, the tissues along the dashed white line are used.

pairs the tissue composition in-between the antennas needs to be investigated. For that purpose the direct connection (the shortest path) between transmitter and receiver is considered. This approach is depicted in Fig. 1 by the solid black line for one transmitter-receiver pair. Each tissue that lies on this line is included into the multi-layered dielectric with its corresponding thickness for this transmitter-receiver pair.

In this way it is assumed that all the transmit power is sent from the transmitter only in the direction of the receiver and not in any other direction. Thus, it is implied that the transmitter knows in which direction the receiver is located. This will not affect the upper bound characteristic of the channel capacity as every real antenna will distribute the power in nearly every spatial direction, leading to a signal with much lower power in the desired direction to the receiver.

In our previous work in [13] and [14] we calculated the frequency dependent path loss only from communication links in horizontal slices of the body model. Afterwards these results were transferred to the 3D model using the probability distribution of the channel capacity. Due to a new algorithm to analyze the tissue composition between the transmitter-receiver pairs, the computation time could be reduced. Hence, the frequency dependent path loss can now be directly computed from the 3D voxel model. This was done to increase the accuracy of our results.

Fig. 2 shows the surface of the body model which was discretized to reduce the number of possible receiver locations on the abdomen. Each rectangle of this discrete surface is about 2 cm × 3 cm in size. The red shaded area shows the abdominal region that was considered. The centroids of each of the 300 red rectangles were used as possible receive antenna locations. The blue dots show all 5000 randomly chosen transmitter locations in the gastrointestinal tract. It was made sure before selecting the points that the smallest distance between any two selected transmitter locations is larger than 4 mm.

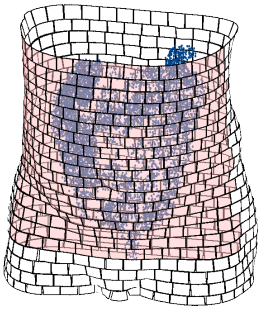

FIGURE 2. The surface of the Visible Human body model. The red shaded area is the abdominal area that was considered for possible receive antenna locations. From each rectangle the centroid was used as receiver location. The blue dots are the transmitter locations in the gastrointestinal tract.

The tissue composition is now analyzed from each transmitter location in the gastrointestinal tract to each of the possible receiver locations, resulting in a total of 1.5×10^6 communication links that are investigated. In Section III it is described in detail how these tissue compositions are used to calculate the frequency dependent path loss of a plane wave traveling through this compound material.

B. LIMIT ON THE TRANSMIT POWER

The transmit power inside the human body is restricted by spectral regulations and the specific absorption rate (SAR) limits defined by the International Commission on Non-Ionizing Radiation Protection (ICNIRP). The SAR limit is defined in a way that the body temperature never increases by more than 1 °C. Including some safety margin, it was set to 2 W/kg averaged over 10 g of tissue [3]. It was shown by simulations in [8] that the SAR limit puts a much higher constraint on the transmit power than the spectral regulations. The spectral mask allowed in ultra wideband radio is −41.3 dBm/MHz. To reach this limit with a transmitter placed in the small intestine, a transmit power of 4.38 W would be needed. However, the limit of the specific absorption rate is already reached for a transmit power of 21.5 mW [8]. As the specific absorption rate depends on the total power transmitted and not on the power density [15], for all following calculations the maximum transmit power will be set to $P_{TX,max} = 21.5$ mW.

C. DIELECTRIC PROPERTIES OF HUMAN TISSUE

The Visible Human voxel model consists of more than 50 different tissue types. Each tissue in the human body is essentially a frequency dependent lossy dielectric. Investigations from Gabriel *et al.* [16] showed that the frequency dependent behavior of the relative permittivity can be modeled by the following Cole-Cole expression:

$$\varepsilon_r(f) = \varepsilon_\infty + \sum_{n=1}^{4} \frac{\Delta\varepsilon_n}{1 + (j2\pi f \tau_n)^{1-\alpha_n}} + \frac{\sigma}{j2\pi f \varepsilon_0}, \qquad (1)$$

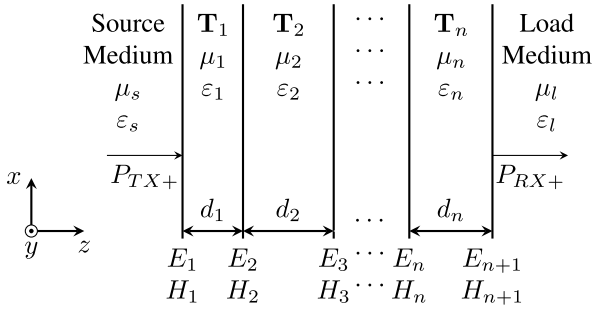

FIGURE 3. A plane wave with power P_{TX+} propagating through a multi-layered dielectric. The wave propagates along the positive z-direction and has a power of P_{RX+} at the receiver.

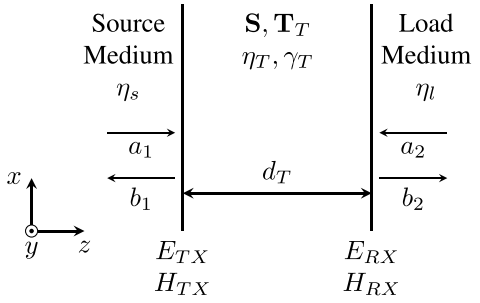

FIGURE 4. Equivalent dielectric of the total tissue composition for the computation of the S-parameters.

where ε_∞ is the permittivity for $f \to \infty$, σ is the conductivity, ε_0 is the permittivity of free-space, f is the frequency, and $\Delta\varepsilon_n$, τ_n, α_n are tissue specific parameters. Details on the parameters can be found in [16]. The relative permeability of human tissue is assumed to be $\mu_r = 1$.

III. FREQUENCY DEPENDENT PATH LOSS OF A MULTI-LAYERED DIELECTRIC

A. FROM TRANSMISSION TO SCATTERING PARAMETERS

The propagation of a plane wave through a multi-layered dielectric, as depicted in Fig. 3, can be described by the transmission matrix $\mathbf{T}$ of the dielectric. The matrix $\mathbf{T}$ gives the relationship between the electric and the magnetic fields at the boundary i to the fields at the boundary $i+1$

$$\begin{bmatrix} E_i \\ H_i \end{bmatrix} = \mathbf{T}_i \begin{bmatrix} E_{i+1} \\ H_{i+1} \end{bmatrix}. \tag{2}$$

For each layer i the transmission matrix $\mathbf{T}_i$ is defined as [11]

$$\mathbf{T}_i = \begin{bmatrix} A_i & B_i \\ C_i & D_i \end{bmatrix} = \begin{bmatrix} \cosh \gamma_i d_i & \eta_i \sinh \gamma_i d_i \\ \frac{1}{\eta_i} \sinh \gamma_i d_i & \cosh \gamma_i d_i \end{bmatrix}, \tag{3}$$

where $\gamma_i = j2\pi f \sqrt{\mu_i \varepsilon_i}$ is the propagation constant, $\eta_i = \sqrt{\mu_i/\varepsilon_i}$ is the wave impedance and d_i is the thickness of the i-th medium. With these definitions the total composition of all n dielectrics can be described by $\mathbf{T}_T = \mathbf{T}_1 \cdot \mathbf{T}_2 \cdots \mathbf{T}_n$.

To calculate the path loss $\frac{P_{RX+}}{P_{TX+}}$, a conversion of the $\mathbf{T}$-matrix into its scattering ($\mathbf{S}$-) parameters is needed. Note that the source and load impedances are not real. For this scenario Theilmann *et al.* derived the necessary conversion formulas in [11]. For a better understanding the derivation is summarized here. Refer to [11] for more details.

The matrix $\mathbf{T}_T$ is converted into its $\mathbf{S}$-parameter representation with power parameters $a_1, a_2, b_1,$ and b_2 as shown in Fig. 4. The power parameters are defined as [11]

$$a_1 = \sqrt{\Re(\eta_s)} H_{TX+} \quad b_1 = \sqrt{\Re(\eta_s)} H_{TX-} \tag{4}$$

$$a_2 = \sqrt{\Re(\eta_l)} H_{RX-} \quad b_2 = \sqrt{\Re(\eta_l)} H_{RX+}, \tag{5}$$

where η_s and η_l are the wave impedances of the source and load medium, respectively. The electric and magnetic field at the boundaries to the source and load medium have been split into a forward and a backward traveling wave $E_{TX} = E_{TX+} + E_{TX-}$ and $H_{TX} = H_{TX+} - H_{TX-}$, likewise for E_{RX} and H_{RX}. The subscripted $+$ indicates a wave traveling in positive z-direction and a $-$ indicates a wave traveling in negative z-direction. Moreover, the following relationship of electric and magnetic field of a plane wave holds[2]:

$$E_{TX+} = \eta_s H_{TX+} \quad E_{TX-} = \eta_s H_{TX-} \tag{6}$$

$$E_{RX+} = \eta_l H_{RX+} \quad E_{RX-} = \eta_l H_{RX-}. \tag{7}$$

Taking (4) to (7) the power parameters are defined in such a way that the squared magnitude of the scattering parameters give the ratio of incoming to outgoing power for the transmission medium. The path loss is then

$$\begin{aligned} \mathrm{PL}(f) = |S_{21}|^2 &= \left| \frac{b_2}{a_1} |_{a_2=0} \right|^2 \\ &= \frac{\frac{1}{2}\Re(\eta_s)\,|E_{RX+}|^2}{\frac{1}{2}\Re(\eta_l)\,|E_{TX+}|^2} = \frac{P_{RX+}}{P_{TX+}}, \end{aligned} \tag{8}$$

where P_{TX+} is the time average power transmitted inside the dielectric from the source medium and P_{RX+} is the power received by a receiver inside the load medium. With these definitions, S_{21} can be expressed in terms of the entries of the $\mathbf{T}_T$-matrix as

$$S_{21} = \frac{\sqrt{\Re(\eta_l)}}{\sqrt{\Re(\eta_s)}} \frac{2\eta_s}{\eta_l A_T + B_T + \eta_l \eta_s C_T + \eta_s D_T}. \tag{9}$$

As the source and load impedance are complex in this case, it has to be noted that in general $S_{21} \neq S_{12}$. This does not influence the electromagnetic reciprocity, only $\mathbf{S}$ is not necessarily symmetric [17].

B. SOURCE AND LOAD IMPEDANCE

The receiver is placed on the body surface, that means the wave impedance of the load medium η_l is always set to the wave impedance of air ($\eta_l = 376.73\,\Omega$). However, the transmitter is placed somewhere in the gastrointestinal tract and, thus, there are reflections occurring from parts of the wave that propagate away from the receiver. These reflection effects will be included in the source impedance.

[2]Note: the conjugate complex that occurs at this point in [11] in equation (A2) should in our opinion not appear there.

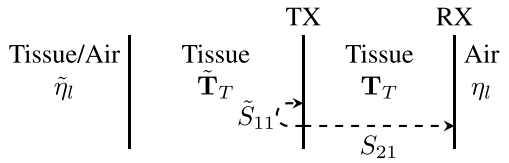

FIGURE 5. Calculation of the source impedance is based on the reflection coefficient $\tilde{S}_{11}$ at the transmitter.

Consider the example depicted in Fig. 1. The tissue through which the wave passes on its way to the receiver lies along the black arrow connecting TX and RX. To include the reflections occurring at the transmitter, the tissues in the opposite of this direction are considered (indicated by the dashed white line in Fig. 1). This idealized setup is shown in Fig. 5. The tissue composition along the opposite propagation direction of the communication signal is denoted by the matrix $\tilde{\mathbf{T}}_T$. With this, the source impedance can be calculated from the reflection coefficient $\tilde{S}_{11}$ as [11]

$$\eta_s = \frac{\tilde{\eta}_l \tilde{A}_T + \tilde{B}_T}{\tilde{\eta}_l \tilde{C}_T + \tilde{D}_T}. \tag{10}$$

Where $\tilde{A}_T$, $\tilde{B}_T$, $\tilde{C}_T$, and $\tilde{D}_T$ are the components of $\tilde{\mathbf{T}}_T$ and $\tilde{\eta}_l$ is the wave impedance of the load material from $\tilde{\mathbf{T}}_T$. As the attenuation of the tissue is very high, the tissue composition $\tilde{\mathbf{T}}_T$ is considered only for a depth of up to 10 cm or until the body surface is reached. Hence, the last tissue type occurring in $\tilde{\mathbf{T}}_T$ is used for the calculation of $\tilde{\eta}_l$.

IV. CHANNEL CAPACITY IN A FREQUENCY-SELECTIVE AWGN CHANNEL

The channel capacity gives an upper limit on the data rate that may be transmitted over a communication channel. As long as the data rate is smaller than the capacity, there exist error correcting codes which theoretically enable communication with an arbitrarily low error rate. However, if the data rate is larger than the capacity, there exist no such codes.

For a real channel with additive white Gaussian noise (AWGN) limited to the frequency band B, the channel capacity in bit/s can be calculated as [18]:

$$C = B \log_2\left(1 + \frac{P_{RX+}}{N}\right) = B \log_2\left(1 + \frac{2 \cdot E_s}{N_0}\right). \tag{11}$$

Where P_{RX+} is the received signal power, N is the noise power, $E_s = \frac{P_{RX+}}{2B}$ the energy per receive symbol, and $\frac{N_0}{2}$ the two-sided noise power spectral density.

In a frequency-selective channel, the capacity can be defined for a small subband Δf around a center frequency f_i. If the path loss $\mathrm{PL}(f)$, the power spectral density of the transmit signal $S_{XX}(f)$, and the power spectral density of the noise $S_{NN}(f)$ are assumed to be constant in this subband, the resulting channel capacity is [18]

$$C(f_i) = \Delta f \log_2\left(1 + \frac{S_{XX}(f_i)\mathrm{PL}(f_i)}{S_{NN}(f_i)}\right). \tag{12}$$

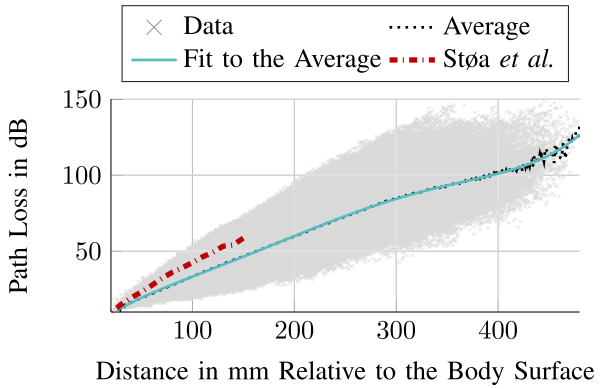

FIGURE 6. The path loss model from Støa *et al.* [7] compared to the data determined from our proposed model and the fit through the average path loss in dB. In both cases the transmission bandwidth was 1 GHz to 6 GHz.

For $\Delta f \to 0$ the total capacity C of the channel yields

$$C = \int_0^\infty \log_2\left(1 + \frac{S_{XX}(f)\mathrm{PL}(f)}{S_{NN}(f)}\right) \mathrm{d}f. \tag{13}$$

As an AWGN channel is assumed, the noise power spectral density is $S_{NN} = \frac{N_0}{2} = \frac{kT}{2} = -156.93\,\mathrm{dBm/Hz}$. The temperature of the receiver was assumed to be $T = 20\,^\circ\mathrm{C}$. Additionally, a noise figure of 20 dB has been considered [2].

V. COMPARISON TO EXISTING CHANNEL MODELS

To validate our results, we compare the resulting path loss from our model in different frequency bands to path loss models from literature. The comparison is limited to those studies which also investigate the ultra wideband propagation behavior in the abdominal region. We split the different available path loss models into two groups for better comparability according to the used bandwidth. The first in the frequency range of 1 GHz to 6 GHz and the second from 3.4 GHz to 4.8 GHz, which is the so-called UWB low band [19].

A. PATH LOSS FOR 1 GHz TO 6 GHz

In Fig. 6 the path loss of all 1.5×10^6 communication links of our model in a frequency range of 1 GHz to 6 GHz is shown by the tiny gray crosses. The path loss was calculated from (8) assuming that the transmit power is uniformly distributed in the frequency range of 1 GHz to 6 GHz. For each distance in steps of 1 mm the average path loss in dB was computed and is shown by the dotted black line in Fig. 6. The light green curve shows a fit through the average path loss, which was found to be well described by

$$\mathrm{PL}_{\mathrm{dB,av}}(d) = \sum_{i=0}^{5} p_i \left(\frac{d}{d_0}\right)^i. \tag{14}$$

The coefficients p_i, which are given in Table 1, were found using curve fitting in MATLAB. The distance d between transmitter and receiver is given in mm in the range of 26 mm

TABLE 1. Coefficients for the fit to the average path loss in dB.

i	p_i	
	1 GHz to 6 GHz	3.4 GHz to 4.8 GHz
5	3.83×10^{-11}	4.726×10^{-11}
4	-4.263×10^{-8}	-5.057×10^{-8}
3	1.679×10^{-5}	1.894×10^{-5}
2	-2.972×10^{-3}	-3.228×10^{-3}
1	0.5035	0.8401
0	−0.2488	−3.786

to 480 mm and $d_0 = 1$ mm. With this fit the RMSE to the mean is 1.2 dB.

Støa *et al.* [7] simulated a plane wave excited by a Gaussian pulse with the finite-difference time-domain (FDTD) method. The pulsed wave was sent onto the body surface in the abdominal region. The pulse had, according to the authors, most of its energy in the frequency range of 1 GHz to 6 GHz. They determined the path loss by evaluating the received power of the plane wave from several hundred ideal electric and magnetic field probes inside the abdomen. As the authors did a FDTD simulation, scattering at the tissue boundaries is included in their model. However, they do not include antenna effects. The average path loss of their model is shown in Fig. 6 with the red-dashed curve.

It can be seen from Fig. 6 that the average path loss from our model is always smaller than the average path loss from Støa *et al.* This was expected, as our model does not include any scattering at tissue boundaries. The plane wave in our model hits the boundaries always perpendicular. Hence, the losses are smaller. The curve of Støa *et al.* is at most 12 dB above our result and well within the range of values that are possible with our model.

B. PATH LOSS FOR 3.4 GHz to 4.8 GHz

In the frequency range 3.4 GHz to 4.8 GHz a total number of three papers could be found. From each path loss model the average path loss is shown in Fig. 7.

Shi *et al.* [6] did a finite-difference time-domain (FDTD) simulation. They simulated the communication of a transmit antenna at 33 different locations in the gastrointestinal tract with a receive antenna at five different locations on the abdomen. The frequency range was set to 3.4 GHz to 4.8 GHz.

Experimental results are reported by Floor *et al.* [10]. The authors measured the path loss from an antenna placed in the abdomen to one on the body surface of an anesthetized pig. They used a vector network analyzer to sweep through the frequency range of 1 GHz to 6 GHz. In Fig. 7 the curve for 4 GHz is shown. It can be seen that the curves from Shi *et al.* and Floor *et al.* coincide very well. However, the result from Thotahewa *et al.* [8] shows a larger attenuation. Thotahewa *et al.* did a FDTD simulation in the frequency range of 3.5 GHz to 4.5 GHz including antenna effects. Nonetheless, their results are approximately 10 dB above the results from the other two

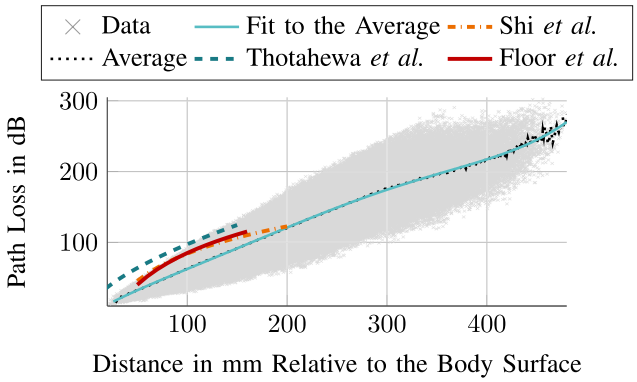

FIGURE 7. The path loss models from Thotahewa *et al.* [8], Floor *et al.* [10], and Shi *et al.* [6] compared with the data and the average path loss in dB from our proposed model for a frequency range of 3.4 GHz to 4.8 GHz.

papers. The reason might be that different antenna models were used.

The results from our model are indicated again with gray crosses in Fig. 7. Additionally, the black dotted curve shows the average of the path loss in dB, that was calculated in steps of 1 mm. The light green curve shows a fit to the average path loss, which can be well approximated with a RMSE of 2.4 dB by (14). The coefficients for this frequency range are given in Table 1.

Due to the fact that all the models from literature include the scattering at tissue boundaries inside the body, it was expected that the path loss of our model underestimates the path loss compared to literature results. The deviation of the model from Thotahewa *et al.* to the one from Shi *et al.* is approximately 10 dB and the deviation from our model to the one from Shi *et al.* is 10 dB to 20 dB. Moreover, our model does not include any antenna effects. This means that the deviation between all path loss models is very similar. Hence, our model provides a similar approximation to the real path loss as other models in literature. Additionally, it is possible using our model to calculate the frequency dependent path loss for a lot more transmitter-receiver pairs than with traditional finite-difference time-domain simulations. Furthermore, our approach allows us to determine the optimum placement of the receive antennas on the body surface. This will be elaborated further in the next section.

VI. DETERMINATION OF THE PLACEMENT OF THE RECEIVE ANTENNAS BASED ON THE CHANNEL CAPACITY

After evaluating the overall statistics of the path loss, this section deals with the distribution of the path loss and the channel capacity on the body surface. First, the placement of only one receive antenna on the body surface is investigated. In the next step multiple antennas employing a selection diversity scheme are evaluated.

In this section a frequency range of 3.1 GHz to 4.8 GHz is considered. This is the so-called UWB low band which is preferable over the higher frequency ranges due to its

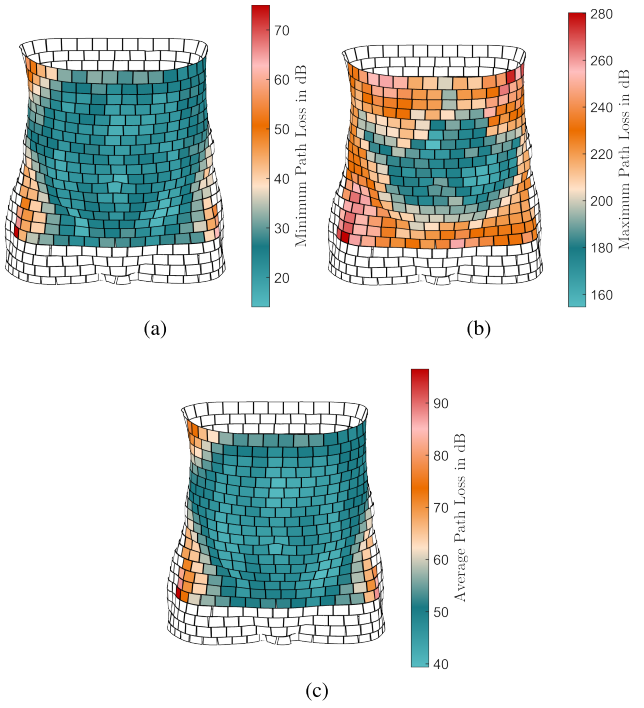

FIGURE 8. The minimum (a), maximum (b), and average (c) path loss for different receiver position on the body surface. The transmitter is passing through all locations in the gastrointestinal tract.

lower attenuation [19]. For all capacity calculations the total transmit power was set to the maximum of 21.5 mW and assumed to be uniformly distributed in the aforementioned frequency range.

A. CHANNEL CAPACITY FOR ONE RECEIVE ANTENNA

In Fig. 8 the path loss distribution on the abdominal surface is shown for one antenna. It shows the discretized body surface of the Visible Human body model. Each rectangle is colored to show the minimum (Fig. 8a), maximum (Fig. 8b), and average (Fig. 8c) path loss at each of these receiver locations for a transmitter passing through all locations in the gastrointestinal tract. It can be seen that the minimum and the average path loss are smallest on the abdomen in a quite large circle around the navel. Moreover, it can be seen from Fig. 8c that on most of the abdomen the average path loss is between 40 dB and 55 dB. However, the maximum path loss in Fig. 8b has a much wider spread from 160 dB to 280 dB and its minimum is only achievable in a comparably small area around the navel.

The main goal of this work is to determine the channel capacity of a link inside the abdominal region using UWB transmission. In the following we use the 10 %-outage capacity as a measure as it is more meaningful than the average capacity under these slow varying channel conditions. The 10 %-outage capacity gives the capacity that is achieved in at least 90 % of all channel realizations. This means in our model the capacity that is achieved for at least 90 % of all transmitter locations in the gastrointestinal tract.

From each transmitter location in the gastrointestinal tract to each receiver location on the body surface the channel capacity is calculated. The 10 %-outage capacity is then determined for each receiver location over all transmitter locations. In Fig. 9 the 10 %-outage capacity is shown on the body surface for one receive antenna. The maximum of 440.7 kbit/s is marked with a white cross. A data rate of 455.4 kbit/s is standardized for narrowband communication in the MICS band. Hence, using only one receive antenna would not improve the data rate compared to the existing narrowband standard. It is clear that by increasing the number of receive antennas and using diversity reception the channel capacity will be improved.

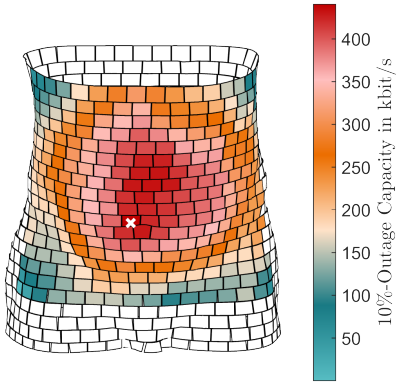

FIGURE 9. The 10 %-outage capacity on the abdominal surface for one receive antenna. The transmitter is passing through all locations in the gastrointestinal tract. The maximum of 440.7 kbit/s is marked with a white cross.

B. CHANNEL CAPACITY FOR MULTIPLE RECEIVE ANTENNAS

If multiple receive antennas are used, there is the need for a diversity scheme to select or combine the received signals. As stated in Section II-A it is assumed in our model that the transmitter knows exactly where the receiver is located. Hence, all the transmit power is sent in that direction. A logical extension for multiple receive antennas is that the transmitter not only knows the direction of the receiver but also the direction of the best receiver (the one with the highest channel capacity), which corresponds to an implementation of selection diversity at the transmitter. Hence, we assume that the transmitter has (by some genie) perfect knowledge about all possible communication channels and selects the one with the best conditions.

The procedure to calculate the maximum 10 %-outage capacity for different numbers of antennas is the following. The channel capacity is calculated from each transmitter location in the gastrointestinal tract to each receiver location on the body surface as in the one antenna case. However, now each combination of N receive antennas out of the 300 possible positions on the abdominal surface is investigated. For each combination of receive antennas only the link with the highest channel capacity from each transmit location is considered. From these capacity values the 10 %-outage channel capacity is calculated. Finally from all these 10 %-outage capacities the maximum is selected as optimum receiver location for each number of antennas.

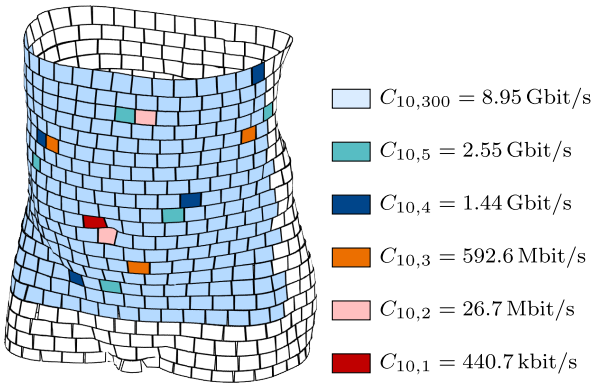

FIGURE 10. Optimum position in terms of maximum 10 %-outage channel capacity of up to five receive antennas operating in a selection diversity scheme. As an upper limit also the capacity for 300 antennas is included.

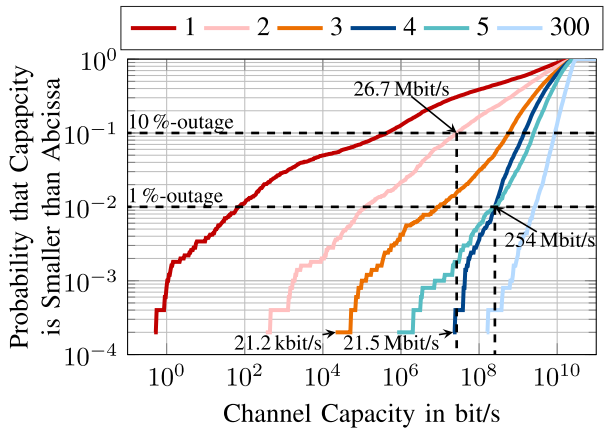

FIGURE 11. Cumulative density function of the channel capacity for each of the optimum positions for different numbers of antennas.

The results for $N = 1, \ldots, 5$ are shown in Fig. 10. As the possible number of combinations grows exponentially it was not possible to investigate more than five different receiver positions. To limit the number of combinations, already for five antennas the minimum distance between any two receiver positions had to be set to 10 cm.

Adding a second receive antenna leads to an increase of the 10 %-outage capacity of nearly 2 orders of magnitude, namely to $C_{10,2} = 26.7$ Mbit/s. For three antennas it increases to 592.6 Mbit/s, for four antennas to 1.44 Gbit/s, and for five antennas to 2.55 Gbit/s.

Up to this point the channel capacity is increasing drastically with every added receive antenna. However, the capacity cannot increase infinitely. For that reason we were interested in the upper limit of this behavior and calculated the channel capacity for $N = 300$ receive antennas, meaning that on each of the discretized locations on the abdomen there was an antenna placed. The 10 %-outage channel capacity is in that case 8.95 Gbit/s. Thus, with five antennas already 28 % of this upper limit is reached.

As can be seen from Fig. 10 the positioning of the antennas is different for different numbers of antennas. However, it seems that one antenna has to be near the navel and the others are somehow uniformly distributed over the abdominal surface with a maximum distance between each other.

In Fig. 11 the cumulative density function (CDF) of the channel capacity for each of the optimum positions depicted in Fig. 10 is shown. It can be seen that not only the 10 %-outage capacity is increasing for a larger number of antennas. It is also visible that the minimum channel capacity is improving. For example the minimum capacity is increasing from 21.2 kbit/s to 21.5 Mbit/s by adding a fourth antenna. That means with four antennas the minimum capacity occurring at all is approximately the same as the 10 %-outage capacity for the two antenna case.

However, the CDF for five antennas intersects with the one for four antennas at a probability of 10^{-2}. Thus, the 1 %-outage channel capacity for four and five antennas is nearly the same ($\approx$254 Mbit/s). That means that the optimum placement of five antennas in terms of 10 %-outage capacity does not necessarily lead to an optimum placement in terms of 1 %-outage capacity.

VII. CONCLUSION

In this work a new approach to model the communication channel for ultra wideband in-body communication is proposed. The basic idea is to model each communication link from a transmitter inside the gastrointestinal tract to an on-body receiver as a multi-layered dielectric. By assuming a plane wave traveling through this compound dielectric, the frequency dependent path loss can be calculated analytically. With the help of the frequency dependent path loss, the channel capacity for each link can be determined.

A comparison to already existing path loss models shows that our proposed model fits well to the ones published in literature so far. The differences that occur can be explained by the fact that scattering at tissue boundaries and antenna effects were not considered in our model.

Our results show that with five antennas placed in their optimum positions a 10 %-outage channel capacity of 2.55 Gbit/s can be achieved. With these five antennas already 28 % of the upper limit for 300 antennas (8.95 Gbit/s) can be reached.

REFERENCES

[1] A. Kiourti, K. A. Psathas, and K. S. Nikita, "Implantable and ingestible medical devices with wireless telemetry functionalities: A review of current status and challenges," *Bioelectromagnetics*, vol. 35, no. 1, pp. 1–15, Jan. 2014.

[2] *IEEE Standard for Local and Metropolitan Area Networks—Part 15.6: Wireless Body Area Networks*, IEEE Standard 802.15.6-2012, 2012.

[3] International Commission on Non-Ionizing Radiation Protection, "Guidelines for limiting exposure to time-varying electric, magnetic and electromagnetic fields (up to 300 GHz)," *Health Phys.*, vol. 74, no. 4, pp. 494–522, 1998.

[4] *Revision of Part 15 of the Commission's Rules Regarding Ultra-Wideband Transmission Systems*, Federal Communications Commission, Washington, DC, USA, 2002.

[5] A. F. Molisch, "Introduction to UWB Signals and Systems," in *Ultra-Wideband: Antennas and Propagation for Communications, Radar and Imaging*, B. Allen, M. Dohler, E. E. Okon, W. Q. Malik, A. K. Brown, and D. J. Edwards, Eds. Chichester, U.K.: Wiley, 2006, pp. 1–17.

[6] J. Shi, D. Anzai, and J. Wang, "Channel modeling and performance analysis of diversity reception for implant UWB wireless link," *IEICE Trans. Commun.*, vol. E95-B, no. 10, pp. 3197–3205, 2012.
[7] S. Støa and R. Chávez-Santiago, and I. Balasingham, "An ultra wideband communication channel model for the human abdominal region," in *Proc. IEEE Globecom Workshops*, Sep. 2010, pp. 246–250.
[8] K. M. S. Thotahewa and J.-M. Redouté, and M. R. Yuce, "Propagation, power absorption, and temperature analysis of UWB wireless capsule endoscopy devices operating in the human body," *IEEE Trans. Microw. Theory Techn.*, vol. 63, no. 11, pp. 3823–3833, Nov. 2015.
[9] D. Anzai *et al.*, "Experimental evaluation of implant UWB-IR transmission with living animal for body area networks," *IEEE Trans. Microw. Theory Techn.*, vol. 62, no. 1, pp. 183–192, Jan. 2014.
[10] P.-A. Floor *et al.*, "In-body to on-body ultrawideband propagation model derived from measurements in living animals," *IEEE J. Biomed. Health Informat.*, vol. 19, no. 3, pp. 938–948, May 2015.
[11] P. Theilmann, M. A. Tassoudji, E. H. Teague, D. F. Kimball, and P. M. Asbeck, "Computationally efficient model for UWB signal attenuation due to propagation in tissue for biomedical implants," *Prog. Electromagn. Res. B*, vol. 38, pp. 1–22, Apr. 2012.
[12] *Virtual Human Database*, Helmholtz Zentrum München, Deutsches Forschungszentrum für Gesundheit und Umwelt, 2016. [Online]. Available: http://www.helmholtz-muenchen.de/amsd/service/scientific-services/virtual-human-database/index.html
[13] J.-C. Brumm and G. Bauch, "Optimum receiver location for ultra wideband in-body communication based on channel capacity calculation," in *Proc. 11th Int. Conf. Body Area Netw.*, Turin, Italy, 2016, pp. 141–147.
[14] J.-C. Brumm and G. Bauch, "Channel capacity and optimum transmission bandwidth of in-body ultra wideband communication links," in *Proc. 11th Int. ITG Conf. Syst. Commun. Coding (SCC)*, Hamburg, Germany, 2017.
[15] J. Wang and Q. Wang, *Body Area Communications: Channel Modeling, Communication Systems, and EMC*. Singapore: Wiley, 2013.
[16] S. Gabriel, R. W. Lau, and C. Gabriel, "The dielectric properties of biological tissues: III. Parametric models for the dielectric spectrum of tissues," *Phys. Med. Biol.*, vol. 41, no. 11, pp. 2271–2293, 1996.
[17] R. B. Marks and D. F. Williams, "A general waveguide circuit theory," *J. Res. Nat. Inst. Standards Technol.*, vol. 97, no. 5, pp. 533–562, Oct. 1992.
[18] J. R. Barry, *Digital Communication*, 3rd ed. Boston, MA, USA: Springer, 2004.
[19] J. Shi and J. Wang, "Channel characterization and diversity feasibility for in-body to on-body communication using low-band UWB signals," in *Proc. 3rd Int. Symp. Appl. Sci. Biomed. Commun. Technol. (ISABEL)*, 2010, pp. 1–4.

JAN-CHRISTOPH BRUMM (S'17) received the B.Sc. and M.Sc. degrees in electrical engineering from the Hamburg University of Technology, Germany, in 2010 and 2013, respectively. He is currently pursuing the Ph.D. degree with the Institute of Communications, Hamburg University of Technology. His main research interests are in the area of wireless communication, in-body signal propagation, and ultra wideband technology.

GERHARD BAUCH (S'99–AM'01–M'03–SM'05–F'15) received the Dipl.-Ing. and Dr.-Ing. degrees in electrical engineering from the Munich University of Technology, in 1995 and 2001, respectively, and the Diplom-Volkswirt (master's in economics) degree from FernUniversitaet Hagen in 2001. In 1996, he was with the German Aerospace Center (DLR), Oberpfaffenhofen, Germany. From 1996 to 2001, he was member of Scientific Staff with the Munich University of Technology. In 1998 and 1999, he was a Visiting Researcher with AT&T Labs Research, Florham Park, NJ, USA. In 2002, he joined DoCoMo Euro-Labs, Munich, Germany, where he has been managing the Advanced Radio Transmission Group. In 2007, he was a additionally appointed Research Fellow with DoCoMo Euro-Labs. From 2003 to 2008, he was an Adjunct Professor with the Munich University of Technology. In 2007, he was a Visiting Professor teaching courses with the University of Udine, in Italy and the Alpen-Adria-University Klagenfurt, in Austria. He was a Full Professor with the Universität der Bundeswehr Munich from 2009 to 2012. Since 2012, he is currently the Head of the Institute of Communications with the Hamburg University of Technology.